Chalcogen isotopes reveal limited volatile contribution from late veneer to Earth

Authors: Wenzhong Wang[1,2*], Michael J. Walter[1], John P. Brodholt[2,3], Shichun Huang[4], Michail I. Petaev[5]

Affiliations:

[1]Earth and Planets Laboratory, Carnegie Institution for Science, Washington, DC 20015, USA

[2]Department of Earth Sciences, University College London, London WC1E 6BT, United Kingdom

[3]Centre for Earth Evolution and Dynamics, University of Oslo, Oslo, Norway

[4]Department of Earth & Planetary Sciences, University of Tennessee at Knoxville, Knoxville, United States

[5]Department of Earth & Planetary Sciences, Harvard University, Cambridge 02138, USA

*Corresponding author. Email: wwang10@carnegiescience.edu & wwz@ustc.edu.cn

Abstract: The origins of Earth's volatiles are highly debated. Comparing the chalcogen isotope ratios in the bulk silicate Earth (BSE) to those of its possible building blocks, chondrites, can be used to constrain the origins of Earth's volatiles; however, this comparison may be complicated by the isotope effects during protoplanetary differentiation, which largely remain poorly understood. Using first-principles calculations, we find that core-mantle differentiation does not significantly fractionate selenium and tellurium isotopes, while equilibrium evaporation from early planetesimals would enrich selenium and tellurium in heavy isotopes in the BSE. The sulfur, selenium, and tellurium isotopic signatures of the BSE reveal that protoplanetary differentiation plays a key role in establishing most of Earth's volatiles and a late veneer does not significantly contribute to the BSE's volatile inventory.

One-Sentence Summary: The Earth obtained its volatiles during its main accretion stage, but not through a patchy veneer arrived late.

Main Text:

Understanding how Earth accreted its volatile elements, particularly its life-essential elements, is key to understanding the planetary evolution and the habitability of terrestrial planets. One group of hypotheses suggests that proto-Earth accreted mainly from nearly volatile-poor materials from the inner Solar system, with subsequent addition of volatile elements supplied by volatile-rich materials from the outer Solar system to the bulk silicate Earth (BSE) after core formation had ceased (*1–4*).

The late-addition model, often referred as a "late veneer", was originally proposed to explain the abundances of highly siderophile elements (HSEs) in the BSE (*5*, *6*), as metal/silicate partitioning indicated their near complete segregation into the metal phase during Earth's core formation (*7*). This model was subsequently adopted to account for chalcogen (sulfur (S), selenium (Se), and tellurium (Te)) abundances in the BSE (*3*) because their concentrations in the Earth's mantle are much higher than expected from their metal/silicate partition coefficients (*8*, *9*). Further, mantle peridotites were found to have chalcogen/HSE abundance ratios similar to those of carbonaceous chondrites, providing evidence for the late delivery of carbonaceous-chondrite-like material to Earth's mantle (*3*), although it remains debated whether the chalcogen/HSE ratios measured in peridotites represent BSE's signatures because of the complicated history of these peridotites (*10*). However, recent experiments suggest that S metal/silicate partition coefficients at core-forming conditions (~20-60 GPa and > 3000 K) (*11*) are much smaller than that at low pressures, and the modeled S abundance in the BSE after core formation could even be higher than the measured value for the Earth's mantle. Thus, a late veneer is not needed to explain the S abundance, and possibly volatile elements more generally, in the BSE.

An alternative possibility is that the proto-Earth accreted from volatile-rich materials, and the present-day volatile element abundances in the BSE was set primarily by protoplanetary differentiation processes including planetesimal evaporation and core formation (*12–14*). Chalcogen isotopes can provide independent constraints on the origin and evolution of Earth's volatile elements. Earth's mantle has a lighter S isotope composition ($\delta^{34}S = [(^{34}S/^{32}S)_{sample}/(^{34}S/^{32}S)_{std}-1]\times1000$ ‰, where std refers to the standard sample) than any type of chondrites (*15*, *16*) (Fig. S1), whereas its Se and Te isotopic compositions ($\delta^{82/76}Se = [(^{82}Se/^{76}Se)_{sample}/(^{82}Se/^{76}Se)_{std}-1]\times1000$ ‰; $\delta^{128/126}Te = [(^{128}Te/^{126}Te)_{sample}/(^{128}Te/^{126}Te)_{std}-1]\times1000$ ‰) are similar to those of carbonaceous chondrites but significantly heavier than those of enstatite chondrites (*17–19*), a postulated dominant isotopic component of Earth's building materials (*20*). The sub-chondritic $\delta^{34}S$ of the BSE, which cannot be a result of a late veneer, is plausibly explained by evaporation from molten planetesimals, with insignificant S isotope fractionation during core formation (*21*). This suggests that protoplanetary differentiation may have played a key role in establishing Earth's volatile element inventory (*12–14*), rather than a late veneer. In contrast, the similarity in $\delta^{82/76}Se$ and $\delta^{128/126}Te$ between the BSE and carbonaceous chondrites was argued to be the result of the late addition of carbonaceous-chondrite-like material to Earth (*17*, *19*). Such a conclusion can be drawn only if protoplanetary differentiation processes did not fractionate Se and Te isotopes. However, Se and Te have cosmochemical and geochemical characteristics similar to S (*22*, *23*), and it is important to assess their isotope fractionation during evaporation and core formation.

We conducted first-principles calculations (see details in Supplementary Materials) to obtain the equilibrium Se and Te isotope fractionation factors between silicate and metal and between vapor and silicate. Selenium and Te are redox-sensitive elements, but there is no literature study investigating the Se and Te species in silicate melts under different redox conditions. By analogy to S, which predominantly occurs as S^{2-} at $\log f\mathrm{O_2}$ < FMQ-1 (1 log unit lower than the fayalite-magnetite-quartz (FMQ) buffer) in silicate melts (*24*, *25*), the Se and Te species are likely dominated by Se^{2-} and Te^{2-} in silicate melts at the $f\mathrm{O_2}$ conditions of core formation for Earth (log $f\mathrm{O_2}$ < FMQ-4) (*26*, *27*), respectively. We model the silicate melts using $Mg_{32}Si_{32}O_{95}Se$, $Mg_{30}NaCa_2Fe_4Si_{24}Al_3H_2O_{89}Se$ (model "pyrolite"), and $Mg_{30}NaCa_2Fe_4Si_{24}Al_3H_2O_{89}Te$ compositions. The metallic melts are modeled by two multicomponent alloys, $Fe_{87}Ni_4Si_{10}C_2O_2H_2S_2Se$ and $Fe_{87}Ni_4Si_{10}C_2O_2H_2S_2Te$.

The structures of Se-bearing melts at 5-100 GPa and 3000 K were derived from first-principles molecular dynamics (FPMD) simulations. The FPMD results show that Se is mainly bonded to Mg and Si atoms in $Mg_{32}Si_{32}O_{95}Se$ melt with a Se-Si distance of 2.25-2.29 Å and a Se-Mg distance of 2.47-2.57 Å (Fig. S2), while it is primarily bonded to Fe atoms with a Se-Fe distance of ~2.2 Å in $Mg_{30}NaCa_2Fe_4Si_{24}Al_3H_2O_{89}Se$ melt (Fig. S3). In $Fe_{87}Ni_4Si_{10}C_2O_2H_2S_2Se$ metallic melt, Se is dominantly bonded to Fe atoms with a Se-Fe distance of 2.20-2.30 Å (Fig. S4). Similarly, Te is also mainly bonded to Fe atoms in $Mg_{30}NaCa_2Fe_4Si_{24}Al_3H_2O_{89}Te$ and $Fe_{87}Ni_4Si_{10}C_2O_2H_2S_2Te$ melts (Fig. S5). The bonding configurations of Se and Te in silicate and metallic melts are similar to those of S under relatively reducing conditions (*21*).

The average force constants, <F>, of Se and Te in melts are controlled by their bonding structures and were calculated using the snapshots from the FPMD simulations based on the harmonic approximation (see Methods). The <F> of Se in $Mg_{32}Si_{32}O_{95}Se$ melt increases from ~ 133 N/m at 5 GPa to ~ 365 N/m at 82 GPa (Fig. S6) because the coordination numbers of Se-Si and Se-Mg bonds significantly increase with pressure (Fig. S2). The <F> of Se in $Mg_{30}NaCa_2Fe_4Si_{24}Al_3H_2O_{89}Se$ melt falls on the <F> vs pressure trend of $Mg_{32}Si_{32}O_{95}Se$ melt, suggesting a negligible compositional effect on <F> of Se in silicate melts (Fig. S6). Similarly, the <F> of Se in the metallic melt increases by ~ 1.6 times from 11 to 100 GPa due to the considerable increase in the coordination number of the Se-Fe bond with compression (Fig. S4). However, the <F> difference between silicate and metallic melts does not significantly change with pressure, which is only 5-25 N/m at 10-80 GPa (Fig. S6). The <F> difference of Te between $Mg_{30}NaCa_2Fe_4Si_{24}Al_3H_2O_{89}Te$ and $Fe_{87}Ni_4Si_{10}C_2O_2H_2S_2Te$ melts is < 10 N/m at ~ 44 GPa. For comparison, the <F> difference of S between the reducing silicate melt and the metallic melt is < 30 N/m at < 80 GPa (*21*).

The equilibrium fractionation value ($10^3\ln\alpha_{\text{silicate-melt}}$) of $^{82/76}$Se and of $^{128/126}$Te between silicate and metallic melts are derived from the <F> differences using the high-temperature approximation of the Bigeleisen-Mayer equation (*28*) (see Supplementary materials). The silicate melt is only marginally enriched in heavy Se and Te isotopes relative to the metallic melt: at 3000 K, the $10^3\ln\alpha_{\text{silicate-metal}}$ of $^{82/76}$Se is < +0.012 ‰ at 10-60 GPa (Fig. 1), and the $10^3\ln\alpha_{\text{silicate-metal}}$ of $^{128/126}$Te is essentially zero at ~44 GPa.

We further model the Se and Te isotope fractionation during Earth's core formation using two endmember models, equilibrium and Rayleigh distillation models. Residual Se and Te abundances in the BSE after core formation are determined by their metal-silicate partition coefficients. Previous experiments (*8*) report a large Se partition coefficient (up to ~120 at 3000 K) between silicate and metal ($D_{Se}^{\text{metal/silicate}}$) at low pressures (< 20 GPa), which is similar to the silicate-metal S partition coefficient ($D_S^{\text{metal/silicate}}$). However, subsequent experiments (*29*) at > 40 GPa suggest that S becomes much less siderophile at Earth's core-forming conditions than previously estimated from extrapolation of low-pressure data (*8*). If this applies to Se,

$D_{Se}^{metal/silicate}$ would also be smaller than the low-pressure data at Earth's core-forming conditions. Accordingly, we use a large range of 30-120 for $D_{Se}^{metal/silicate}$. Our results show that core-mantle differentiation can only shift the BSE's $\delta^{82/76}$Se by at most +0.01 ‰ and +0.05 ‰ for equilibrium and Rayleigh distillation models (Fig. 1), respectively, indicating that core formation cannot explain the BSE's $\delta^{82/76}$Se if Earth accreted predominantly from enstatite-chondrite-like material (*20*). Similarly, core formation can only shift the BSE's $\delta^{128/126}$Te by at most +0.005 ‰ even if $D_{Te}^{metal/silicate}$ is ~ 300 and δ^{34}S by < +0.1 ‰ (*21*), which cannot explain the δ^{34}S difference between the BSE and enstatite chondrites.

We now consider the effect of evaporative loss from molten planetesimals that formed proto-Earth. Previous studies (*30*, *31*) suggest that the net isotope fractionation between vapor and melt during planetesimal evaporation strongly depends on the evaporative conditions (*30*), e.g., the vapor pressure or the vapor saturation degree. If the vapor saturation degree is far lower than 100%, the kinetic effect dominates the net isotope fractionation (*30*, *31*), and the residual melt is always enriched in heavy isotopes after evaporation. This might plausibly explain the heavy $^{82/76}$Se ratio in the BSE relative to the enstatite-chondrite-like material (*17*), but it cannot explain the BSE's negative δ^{34}S value relative to chondrites (*15*, *16*). When planetesimals undergo evaporation in the presence of nebular H_2 under a total pressure of ~ 10^{-4} bar, the vapor saturation degree approaches 100%, and the net isotope fractionation is equal to the equilibrium isotope fractionation between vapor and melt ($10^3\ln\alpha_{vapor\text{-}silicate}$) (*30*, *31*). Our previous thermodynamic calculations using the GRAINS code show that S mainly occurs as H_2S in the vapor phase (Fig. 2), which is enriched in heavy S isotopes relative to the silicate melt (*21*). Modeling indicates that the sub-chondritic δ^{34}S signature in the BSE can be explained by the evaporative loss of ~ 90% S mainly as H_2S from molten planetesimals due to the positive $10^3\ln\alpha_{vapor\text{-}silicate}$ of S isotopes (Fig. 2d).

Following the framework for S isotopes, we conducted thermodynamic calculations with solar abundances (*22*) under $1e^{-4}$ bar using GRAINS to determine the Se and Te species in the vapor phase. The results show that Se in the vapor phase mainly occurs as atomic Se (g), whose fraction increases from ~ 83% at 1300 K to ~ 97% at 1500 K (Fig. 2a). The dominant species for Te in the vapor phase is also atomic Te (g), whose fraction is > 99% at 1300-1500 K. In contrast, S in the vapor phase mainly occurs as H_2S (g) and/or HS (g) at 1300-1500 K (Fig. 2b). The different species for Se and S in the vapor phase reflect a higher electronegativity for S, leading to a negative Gibbs free energy of formation of H_2S (g), whereas the Gibbs free energy of formation is positive for H_2Se (g) and H_2Te (g) (Fig. S7). That is, at 1300-1500 K and 10^{-4} bar total pressure, H_2S (g) is a stable phase, but H_2Se (g) and H_2Te (g) are not. We also conducted thermodynamic simulations with solar elemental abundances but the H concentration decreased by one order of magnitude, which corresponds to a more oxidizing condition than the solar nebula. The results show that the fractions of major Se and Te species in the vapor phase do not significantly change compared with the foregoing case.

To determine the $10^3\ln\alpha_{vapor\text{-}silicate}$, we conducted first-principles calculations to derive the <F> in all species and estimated the <F> in the vapor phase based on their fractions. The vapor phase is enriched in light Se and Te isotopes relative to the silicate melt with the $10^3\ln\alpha_{vapor\text{-}silicate}$ of $^{82/76}$Se ranging from -0.1 to -0.2 ‰ and the $10^3\ln\alpha_{vapor\text{-}silicate}$ of $^{128/126}$Te from -0.031 to -0.023 ‰ at 1300-1500 K (Fig. 2c and Fig. S8). Thus, Se and Te isotopes show an opposite fractionation direction to that of S (Fig. 2d), such that evaporative loss of S, Se, and Te from molten planetesimals will enrich the residual melt with light S isotopes but heavy Se and Te isotopes.

Combining the isotope fractionation data from our study and the literature metal/silicate partition coefficients (*8*, *9*, *29*), we model the abundances and isotopic compositions of S, Se, and Te in the BSE after early planetesimal evaporation followed by late-stage core formation. The Earth's building material, which is required to estimate the initial abundances and isotopic compositions of S, Se, and Te, remains highly debated. Dauphas (2017) (*20*) modeled the isotopic evolution of multi-elements (including O, Ca, Ti, Cr, Ni, Mo, Ru, and Nd) of the Earth's mantle during Earth's accretion and found that the accreted material is mainly characterized by the enstatite-chondrite-like composition with only minor fractions of carbonaceous chondrite-like material. The best-fitting model of Earth's accreting material that can reproduce most of these isotopic signatures consists of 71% enstatite chondrite, 24% ordinary chondrite, and 5% carbonaceous chondrite (*20*). That is, the Earth's accreting materials come from both CC (carbonaceous) and NC (non-carbonaceous) reservoirs, which is also supported by Earth's nucleosynthetic K and Zn isotope anomalies (*32*–*35*). Furthermore, the mass-independent Mo and Nd isotopic composition of Earth's mantle may reflect a mixture between NC and unsampled *s*-process-enriched CC material compared to known chondrites (*36*–*38*), consistent with the Dauphas's model. In contrast, Schiller et al. (2020) found that the mass-independent μ^{54}Fe of Earth's mantle is lower than other chondrites but only overlaps with the value of CI chondrite (*39*), indicating that most of Fe in Earth's mantle derived from inward-drifting CI-like material. If so, large fractions of Cr and Ni in Earth's mantle would be delivered by the same material as Fe is intermediate in metal affinity between Cr and Ni, which, however, cannot explain Earth's Ni and Cr isotopic signatures (*40*–*43*). Overall, we use the Dauphas's model in this study due to the isotopic similarity of Earth and this model for many elements.

The initial $\delta^{34/32}$S, $\delta^{82/76}$Se, and $\delta^{128/126}$Te of Earth's building material are estimated to be ~ -0.21 ‰, -0.35 ‰, and +0.02 ‰, respectively. The initial S, Se, and Te abundances in the accreting material are ~ 4.5 wt%, 20 ppm (*3*), and 1.8 ppm (*18*, *19*), respectively. Our models show that approximately 85 to 95% early evaporative loss can reproduce the present-day BSE's $\delta^{34/32}$S, $\delta^{82/76}$Se, and $\delta^{128/126}$Te, as well as the S, Se, and Te abundances after core formation over the modeled $D_{S}^{metal/silicate}$, $D_{Se}^{metal/silicate}$, and $D_{Te}^{metal/silicate}$ ranges, without the need for a late veneer (Fig. 3).

If the evaporative loss of S, Se, and Te is greater than 95%, the BSE would have S, Se, and Te abundances lower than the present-day BSE's values after core formation, and its $\delta^{34/32}$S, $\delta^{82/76}$Se, and $\delta^{128/126}$Te would deviate from the current BSE's values. In this case, a late veneer is required to increase the S, Se, and Te abundances to the level of the current BSE, but the final $\delta^{34/32}$S, $\delta^{82/76}$Se and $\delta^{128/126}$Te of the BSE would also be affected by the late-veneer material. To evaluate the late-veneer effect on the $\delta^{34/32}$S, $\delta^{82/76}$Se, and $\delta^{128/126}$Te of the bulk silicate reservoir, we conduct Monte Carlo simulations with a late veneer characterized by carbonaceous-chondrite-like material. The models show that the $\delta^{82/76}$Se and $\delta^{128/126}$Te of the BSE can always be reproduced, no matter how much Se and Te in the present-day BSE was added by a late veneer (Fig. S9). However, the $\delta^{34/32}$S of the BSE will be close to the late-veneer value if the amount of S added by the late veneer is too high, and no more than ~30% of the present-day BSE's S budget is allowed to be added by the late veneer to reproduce the BSE's $\delta^{34/32}$S (Fig. S9).

Our modeling suggests that the abundances and isotope compositions of S, Se, and Te in the BSE can be explained by protoplanetary differentiation rather than a late veneer. Even though a late veneer is allowed, the amounts of S, Se, and Te added by the late veneer should not exceed ~30% of the present-day BSE's budgets. If the late veneer volatile-rich material is sourced from the outer Solar System, e.g., carbonaceous chondrite (*1*–*4*), our result constrains that the mass of late veneer cannot exceed 0.2% of the mass of Earth's mantle. This allows an estimate of the maximum budgets of other volatile elements delivered along with chalcogens by the late veneer. Using the elemental abundances in carbonaceous chondrite (*3*, *44–46*) and the BSE (*47*), we find that the late veneer contributes at most 5% of the H and 40% of the C in the current BSE (*45*, *47–49*). The limited amount of water from a late veneer indicates that Earth may have obtained most of its water during early accretion and differentiation (*50*) from its major building block – enstatite-chondrite-like material (*20*) and/or through the interaction between primordial hydrogen atmosphere and proto-Earth. Also, the allowed mass of late veneer would not significantly contribute to the budgets of moderately volatile elements in the BSE, which is supported by the mass-dependent Zn and Cu isotopic signatures of Earth's mantle (*51*, *52*). In contrast, the maximum mass of late veneer constrained from S, Se, and Te isotopes can supply 100% of the N in the current BSE (2.2 ± 1.2 ppm, (*45*, *47*, *53*)). The pre-late veneer BSE would have a higher C/N ratio than the present-day BSE, which is also supported by metal-silicate partition coefficients (*14*, *54*). In addition, at most 30% of the HSEs in the current BSE were added by a late veneer. This is consistent with recent experiments (*55*, *56*) yielding low metal-silicate partition coefficients for Pd and Pt and hinting for possible higher concentrations of platinum-group elements in the mantle after core formation. Overall, our results show that protoplanetary differentiation may play a dominant role in establishing Earth's most volatile element inventory, and the late veneer would have a limited contribution to the BSE's volatiles, with the exception of N.

References and Notes

1. M. Schonbachler, R. W. Carlson, M. F. Horan, T. D. Mock, E. H. Hauri, Heterogeneous Accretion and the Moderately Volatile Element Budget of Earth. *Science (80-.)*. **328**, 884–887 (2010).
2. N. Braukmüller, F. Wombacher, C. Funk, C. Münker, Earth's volatile element depletion pattern inherited from a carbonaceous chondrite-like source. *Nat. Geosci.* **12**, 564–568 (2019).
3. Z. Wang, H. Becker, Ratios of S, Se and Te in the silicate Earth require a volatile-rich late veneer. *Nature*. **499**, 328–331 (2013).
4. M. Fischer-Gödde, T. Kleine, Ruthenium isotopic evidence for an inner Solar System origin of the late veneer. *Nature*. **541**, 525–527 (2017).
5. C.-L. Chou, Fractionation of siderophile elements in the Earths upper mantle. *Proc. Lunar Planet. Sci. Conf. 9th*. **1**, 219–230 (1978).
6. H. Becker, M. F. Horan, R. J. Walker, S. Gao, J.-P. Lorand, R. L. Rudnick, Highly siderophile element composition of the Earth's primitive upper mantle: Constraints from new data on peridotite massifs and xenoliths. *Geochim. Cosmochim. Acta*. **70**, 4528–4550 (2006).
7. U. Mann, D. J. Frost, D. C. Rubie, H. Becker, A. Audétat, Partitioning of Ru, Rh, Pd, Re, Ir and Pt between liquid metal and silicate at high pressures and high temperatures - Implications for the origin of highly siderophile element concentrations in the Earth's mantle. *Geochim. Cosmochim. Acta*. **84**, 593–613 (2012).

8. L. Rose-Weston, J. M. Brenan, Y. Fei, R. A. Secco, D. J. Frost, Effect of pressure, temperature, and oxygen fugacity on the metal-silicate partitioning of Te, Se, and S: Implications for earth differentiation. *Geochim. Cosmochim. Acta*. **73**, 4598–4615 (2009).

9. A. Boujibar, D. Andrault, M. A. Bouhifd, N. Bolfan-Casanova, J. L. Devidal, N. Trcera, Metal-silicate partitioning of sulphur, new experimental and thermodynamic constraints on planetary accretion. *Earth Planet. Sci. Lett.* **391**, 42–54 (2014).

10. A. Yierpan, S. König, J. Labidi, R. Schoenberg, Selenium isotope and S-Se-Te elemental systematics along the Pacific-Antarctic ridge: Role of mantle processes. *Geochim. Cosmochim. Acta*. **249**, 199–224 (2019).

11. R. A. Fischer, Y. Nakajima, A. J. Campbell, D. J. Frost, D. Harries, F. Langenhorst, N. Miyajima, K. Pollok, D. C. Rubie, High pressure metal–silicate partitioning of Ni, Co, V, Cr, Si, and O. *Geochim. Cosmochim. Acta*. **167**, 177–194 (2015).

12. C. A. Norris, B. J. Wood, Earth's volatile contents established by melting and vaporization. *Nature*. **549**, 507–510 (2017).

13. D. S. Grewal, R. Dasgupta, T. Hough, A. Farnell, Rates of protoplanetary accretion and differentiation set nitrogen budget of rocky planets. *Nat. Geosci.* **14**, 369–376 (2021).

14. R. A. Fischer, E. Cottrell, E. Hauri, K. K. M. Lee, M. Le Voyer, The carbon content of Earth and its core. *Proc. Natl. Acad. Sci.* **117**, 8743–8749 (2020).

15. J. Labidi, P. Cartigny, M. Moreira, Non-chondritic sulphur isotope composition of the terrestrial mantle. *Nature*. **501**, 208–211 (2013).

16. J. Labidi, P. Cartigny, C. Hamelin, M. Moreira, L. Dosso, Sulfur isotope budget (32S,33S,34S and36S) in Pacific-Antarctic ridge basalts: A record of mantle source heterogeneity and hydrothermal sulfide assimilation. *Geochim. Cosmochim. Acta*. **133**, 47–67 (2014).

17. M. I. Varas-Reus, S. König, A. Yierpan, J.-P. Lorand, R. Schoenberg, Selenium isotopes as tracers of a late volatile contribution to Earth from the outer Solar System. *Nat. Geosci.* **12**, 779–782 (2019).

18. J. L. Hellmann, T. Hopp, C. Burkhardt, T. Kleine, Origin of volatile element depletion among carbonaceous chondrites. *Earth Planet. Sci. Lett.* **549**, 116508 (2020).

19. J. L. Hellmann, T. Hopp, C. Burkhardt, H. Becker, M. Fischer-Gödde, T. Kleine, Tellurium isotope cosmochemistry: Implications for volatile fractionation in chondrite parent bodies and origin of the late veneer. *Geochim. Cosmochim. Acta*. **309**, 313–328 (2021).

20. N. Dauphas, The isotopic nature of the Earth's accreting material through time. *Nature*. **541**, 521–524 (2017).

21. W. Wang, C. H. Li, J. P. Brodholt, S. Huang, M. J. Walter, M. Li, Z. Wu, F. Huang, S. J. Wang, Sulfur isotopic signature of Earth established by planetesimal volatile evaporation. *Nat. Geosci.* **14**, 806–811 (2021).

22. K. Lodders, Solar System Abundances and Condensation Temperatures of the Elements. *Astrophys. J.* **591**, 1220–1247 (2003).

23. B. J. Wood, D. J. Smythe, T. Harrison, The condensation temperatures of the elements: A reappraisal. *Am. Mineral.* **104**, 844–856 (2019).

24. W. M. Nash, D. J. Smythe, B. J. Wood, Compositional and temperature effects on sulfur speciation and solubility in silicate melts. *Earth Planet. Sci. Lett.* **507**, 187–198 (2019).

25. P. J. Jugo, M. Wilke, R. E. Botcharnikov, Sulfur K-edge XANES analysis of natural and synthetic basaltic glasses: Implications for S speciation and S content as function of oxygen fugacity. *Geochim. Cosmochim. Acta*. **74**, 5926–5938 (2010).

26. M. Wadhwa, Redox Conditions on Small Bodies, the Moon and Mars. *Rev. Mineral. Geochemistry*. **68**, 493–510 (2008).

27. J. Wade, B. J. Wood, Core formation and the oxidation state of the Earth. *Earth Planet. Sci. Lett.* **236**, 78–95 (2005).

28. J. Bigeleisen, M. G. Mayer, Calculation of Equilibrium Constants for Isotopic Exchange Reactions. *J. Chem. Phys.* **15**, 261 (1947).

29. T.-A. Suer, J. Siebert, L. Remusat, N. Menguy, G. Fiquet, A sulfur-poor terrestrial core inferred from metal–silicate partitioning experiments. *Earth Planet. Sci. Lett.* **469**, 84–97 (2017).

30. E. D. Young, A. Shahar, F. Nimmo, H. E. Schlichting, E. A. Schauble, H. Tang, J. Labidi, Near-equilibrium isotope fractionation during planetesimal evaporation. *Icarus*. **323**, 1–15 (2019).

31. H. Tang, E. D. Young, Evaporation from the Lunar Magma Ocean Was Not the Mechanism for Fractionation of the Moon's Moderately Volatile Elements. *Planet. Sci. J.* **1**, 49 (2020).

32. R. Martins, S. Kuthning, B. J. Coles, K. Kreissig, M. Rehkämper, Nucleosynthetic isotope anomalies of zinc in meteorites constrain the origin of Earth's volatiles. *Science (80-.).* **379**, 369–372 (2023).

33. N. X. Nie, D. Wang, Z. A. Torrano, R. W. Carlson, C. M. O'D. Alexander, A. Shahar, Meteorites have inherited nucleosynthetic anomalies of potassium-40 produced in supernovae. *Science (80-.).* **379**, 372–376 (2023).

34. T. Steller, C. Burkhardt, C. Yang, T. Kleine, Nucleosynthetic zinc isotope anomalies reveal a dual origin of terrestrial volatiles. *Icarus*. **386**, 115171 (2022).

35. P. S. Savage, F. Moynier, M. Boyet, Zinc isotope anomalies in primitive meteorites identify the outer solar system as an important source of Earth's volatile inventory. *Icarus*. **386**, 115172 (2022).

36. J. Render, M. Fischer-Gödde, C. Burkhardt, T. Kleine, The cosmic molybdenum-neodymium isotope correlation and the building material of the Earth. *Geochemical Perspect. Lett.* **3**, 170–178 (2017).

37. G. Budde, C. Burkhardt, T. Kleine, Molybdenum isotopic evidence for the late accretion of outer Solar System material to Earth. *Nat. Astron.* **3**, 736–741 (2019).

38. S. Johnston, A. Brandon, C. McLeod, K. Rankenburg, H. Becker, P. Copeland, Nd isotope variation between the Earth–Moon system and enstatite chondrites. *Nature*. **611**, 501–506 (2022).

39. M. Schiller, M. Bizzarro, J. Siebert, Iron isotope evidence for very rapid accretion and differentiation of the proto-Earth. *Sci. Adv.* **6**, 1–8 (2020).

40. T. Hopp, N. Dauphas, F. Spitzer, C. Burkhardt, T. Kleine, Earth's accretion inferred from iron isotopic anomalies of supernova nuclear statistical equilibrium origin. *Earth Planet. Sci. Lett.* **577**, 117245 (2022).

41. A. Trinquier, J. Birck, C. J. Allegre, Widespread 54 Cr Heterogeneity in the Inner Solar System. *Astrophys. J.* **655**, 1179–1185 (2007).

42. S.-J. Wang, W. Wang, J. Zhu, Z. Wu, J. Liu, G. Han, F. Teng, S. Huang, H. Wu, Y. Wang, G. Wu, W. Li, Nickel isotopic evidence for late-stage accretion of Mercury-like differentiated planetary embryos. *Nat. Commun.* **12**, 294 (2021).

43. L. Qin, C. M. O. D. Alexander, R. W. Carlson, M. F. Horan, T. Yokoyama, Contributors to chromium isotope variation of meteorites. *Geochim. Cosmochim. Acta*. **74**, 1122–1145 (2010).

44. N. Braukmüller, F. Wombacher, D. C. Hezel, R. Escoube, C. Münker, The chemical composition of carbonaceous chondrites: Implications for volatile element depletion, complementarity and alteration. *Geochim. Cosmochim. Acta*. **239**, 17–48 (2018).

45. M. M. Hirschmann, Comparative deep Earth volatile cycles: The case for C recycling from exosphere/mantle fractionation of major (H2O, C, N) volatiles and from H2O/Ce, CO2/Ba, and CO2/Nb exosphere ratios. *Earth Planet. Sci. Lett.* **502**, 262–273 (2018).

46. C. M. O. Alexander, R. Bowden, M. L. Fogel, K. T. Howard, C. D. K. Herd, L. R. Nittler, The Provenances of Asteroids, and Their Contributions to the Volatile Inventories of the Terrestrial Planets. *Science (80-.).* **337**, 721–723 (2012).

47. H. Palme, H. S. C. O'Neill, in *Treatise on Geochemistry* (Elsevier, ed. 2, 2014; http://dx.doi.org/10.1016/B978-0-08-095975-7.00201-1), vol. 3, pp. 1–39.

48. W. Wang, M. J. Walter, Y. Peng, S. Redfern, Z. Wu, Constraining olivine abundance and water content of the mantle at the 410-km discontinuity from the elasticity of olivine and wadsleyite. *Earth Planet. Sci. Lett.* **519**, 1–11 (2019).

49. W. Wang, H. Zhang, J. P. Brodholt, Z. Wu, Elasticity of hydrous ringwoodite at mantle conditions: Implication for water distribution in the lowermost mantle transition zone. *Earth Planet. Sci. Lett.* **554**, 116626 (2020).

50. W. Wang, Y. Li, J. P. Brodholt, L. Vočadlo, M. J. Walter, Z. Wu, Strong shear softening induced by superionic hydrogen in Earth's inner core. *Earth Planet. Sci. Lett.* **568**, 117014 (2021).

51. P. A. Sossi, O. Nebel, H. S. C. O'Neill, F. Moynier, Zinc isotope composition of the Earth and its behaviour during planetary accretion. *Chem. Geol.* **477**, 73–84 (2018).

52. P. S. Savage, F. Moynier, H. Chen, G. Shofner, J. Siebert, J. Badro, I. S. Puchtel, Copper isotope evidence for large-scale sulphide fractionation during Earth's differentiation. *Geochemical Perspect. Lett.* **1**, 53–64 (2015).

53. B. Marty, The origins and concentrations of water, carbon, nitrogen and noble gases on Earth. *Earth Planet. Sci. Lett.* **313–314**, 56–66 (2012).

54. D. S. Grewal, R. Dasgupta, C. Sun, K. Tsuno, G. Costin, Delivery of carbon, nitrogen, and sulfur to the silicate Earth by a giant impact. *Sci. Adv.* **5**, eaau3669 (2019).

55. K. Righter, M. Humayun, L. Danielson, Partitioning of palladium at high pressures and temperatures during core formation. *Nat. Geosci.* **1**, 321–323 (2008).

56. T.-A. Suer, J. Siebert, L. Remusat, J. M. D. Day, S. Borensztajn, B. Doisneau, G. Fiquet, Reconciling metal–silicate partitioning and late accretion in the Earth. *Nat. Commun.* **12**, 2913 (2021).

Acknowledgments: W. W. acknowledges support from the UCL-Carnegie Postdoctoral Scholarship. S.H. acknowledge support from NSF AST-1910955 and EAR-2244895. First-principles calculations were conducted at the Supercomputing Center of the University of Science and Technology of China. We thank Bruce Fegley for constructive discussion.

Author contributions: W.W. conceived and designed this project. W.W. performed first-principles calculations and did the GRAINS calculations with the help of M.I.P.. W.W. wrote the manuscript and all authors contributed to the discussion of the results and revision of the manuscript.

Competing interests: The authors declare no competing interests.

Data and materials availability: All data are available in the main text or the supplementary materials. The Vienna Ab Initio Simulation Package is a proprietary software available for purchase at https://www.vasp.at/.

Supplementary Materials

Materials and Methods

Supplementary Text

Figs. S1 to S9

References (*41–53*)

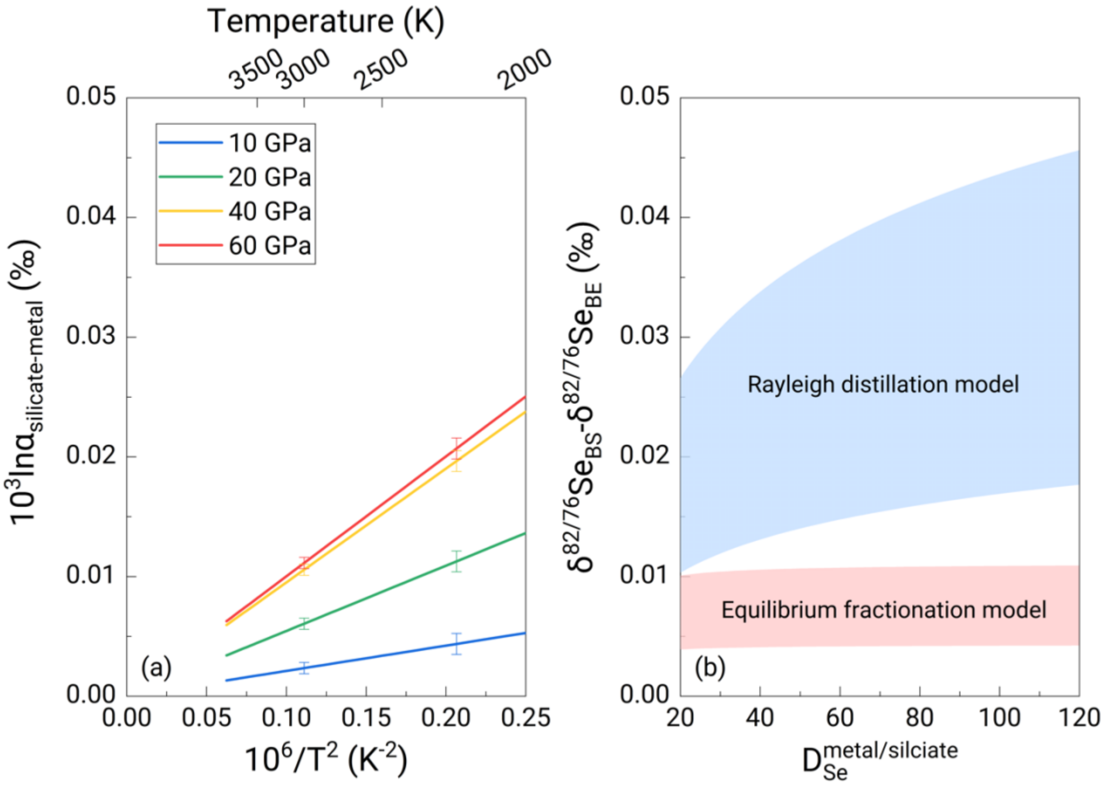

Fig. 1. Selenium isotope fractionation during core formation. (a) Equilibrium Se isotope fractionation factors (10^3lnα of $^{82/76}$Se) between silicate and metallic melts. (b) Modelled $\delta^{82/76}$Se difference between the bulk silicate part ($\delta^{82/76}Se_{BS}$) and the bulk Earth ($\delta^{82/76}Se_{BE}$) caused by mantle-core differentiation. The Se partition coefficient ($D_{Se}^{metal/silicate}$) determines the remaining Se fraction in the silicate part after core formation. Equilibrium and Rayleigh distillation models are considered as two endmember models.

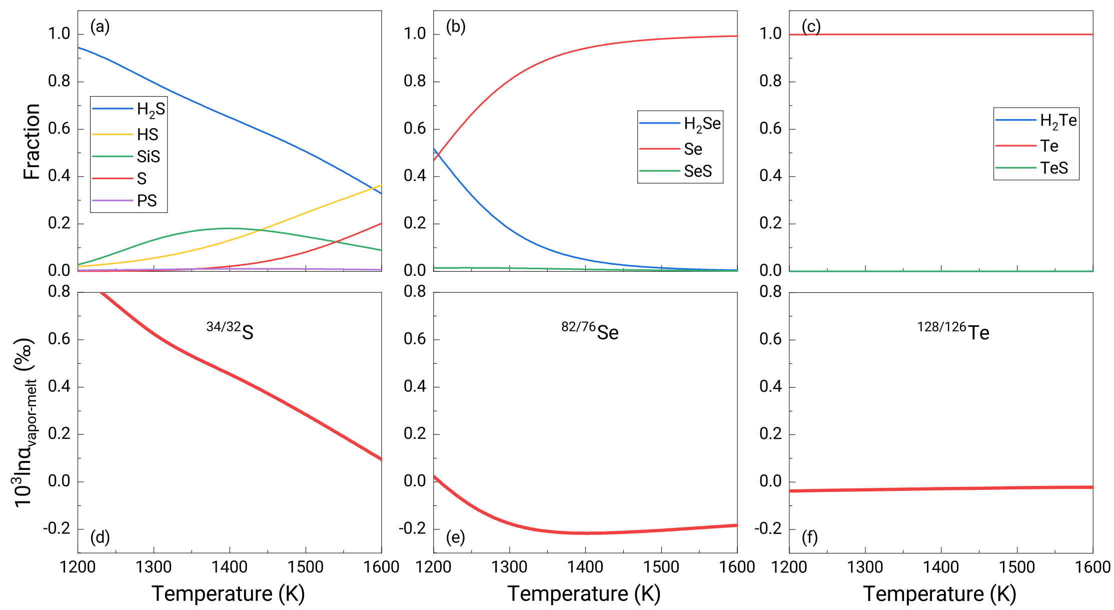

Fig. 2. Sulfur, selenium, and tellurium species in the vapor phase and the isotope fractionation between vapor and melt. (a) (b) (c) the fractions of S, Se, and Te species in the vapor evaporated from molten planetesimals with the presence of nebular H_2. At 1300-1500 K, Se and Te predominantly occur as Se (g) and Te (g), respectively, while S mainly occurs as H_2S (g). (d) (e) (f) the equilibrium S, Se, and Te isotope fractionation factors between vapor and melt. The residual melt is enriched in light S isotopes but heavy Se and Te isotopes relative to the vapor phase due to the different species of S, Se, and Te in the vapor phase.

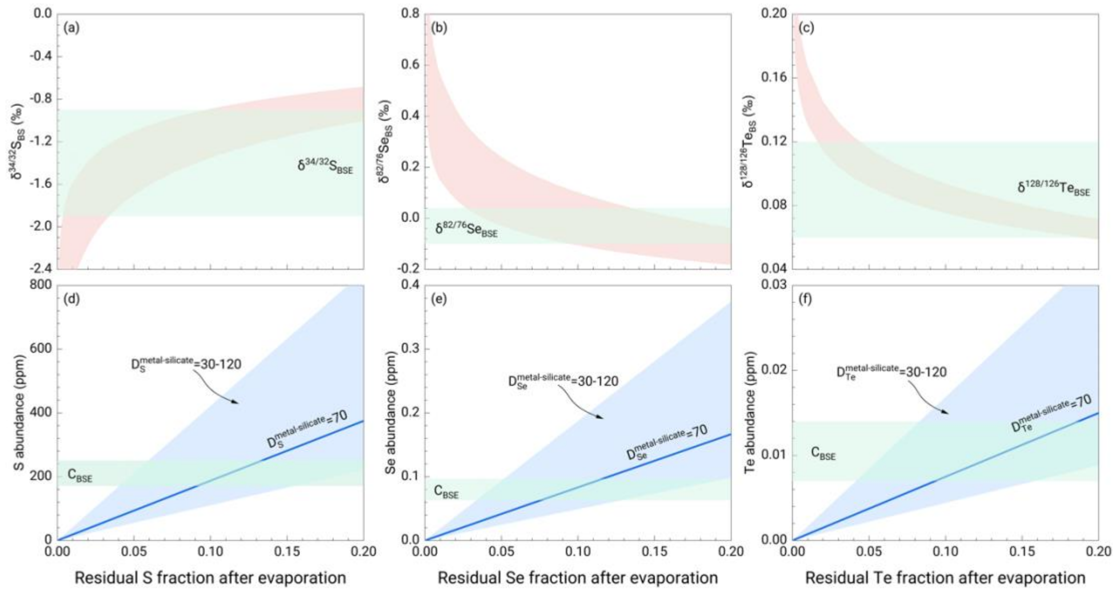

Fig. 3. Abundances and isotopic compositions of S, Se, and Te in the bulk silicate part established by planetesimal evaporation followed by core formation. The green shades refer to the present-day BSE values (*3*, *15–17*, *19*). The Se and Te isotopic compositions of the BSE were inferred from mantle peridotites (*17*, *19*). The previous estimate of BSE's $\delta^{82/76}$Se from Mid-Ocean-Ridge Basalts (*10*) is consistent with the value from peridotites. (a) $\delta^{34/32}S_{BS}$ (b) $\delta^{82/76}Se_{BS}$ and (c) $\delta^{128/126}Te_{BS}$ as a function of the residual fraction after evaporation, as core formation does not induce resolvable S, Se, and Te isotope fractionation. The initial $\delta^{34/32}$S, $\delta^{82/76}$Se, and $\delta^{128/126}$Te of the building material (71% enstatite chondrite + 24% ordinary chondrite + 5% carbonaceous chondrite) (*20*) are estimated to be ~ -0.21 ‰, -0.35 ‰, and +0.02 ‰ (Fig. S1), respectively. (d) S (e) Se (f) Te abundances in the bulk silicate part after evaporation followed by core-mantle differentiation. The initial S, Se, and Te abundances in the build material are set as ~ 4.5 wt%, 20 ppm (*3*), and 1.8 ppm (*18*, *19*), respectively. The blue shades represent the modeled results with $D_S^{metal/silicate}$, $D_{Se}^{metal/silicate}$, and $D_{Te}^{metal/silicat}$ ranging from 30 to 120 (*8*, *9*, *29*), in which the results at $D_S^{metal/silicate}$, $D_{Se}^{metal/silicate}$, and $D_{Te}^{metal/silicate}$ ~ 70 are highlighted by the blue lines.